

Deep Switching State Space Model for Nonlinear Time Series Forecasting with Regime Switching

Xiuqin Xu, Hanqiu Peng, and Ying Chen^a

^a*Department of Mathematics, Asian Institute of Digital Finance, and Risk Management Institute, National University of Singapore, 21 Lower Kent Ridge Rd, 119077, Singapore*

Abstract

Modern time series data often display complex nonlinear dependencies along with irregular regime-switching behaviors. These features present technical challenges in modeling, inference, and providing insightful understanding of the underlying stochastic phenomena. To tackle these challenges, we introduce the novel Deep Switching State Space Model (DS³M). In DS³M, the architecture employs discrete latent variables to represent regimes and continuous latent variables to account for random driving factors. By melding a Recurrent Neural Network (RNN) with a nonlinear Switching State Space Model (SSSM), we manage to capture the nonlinear dependencies and irregular regime-switching behaviors, governed by a Markov chain and parameterized using multilayer perceptrons. We validate the DS³M through short- and long-term forecasting on a wide array of simulated and real-world datasets, spanning sectors such as healthcare, economics, traffic, meteorology, and energy. Our results reveal that DS³M outperforms several state-of-the-art models in terms of forecasting accuracy, while providing meaningful regime identifications.

Keywords: Time Series Forecasting, Nonlinear State Space Models, Deep Learning, Stochastic Regime-Switching, Recurrent Neural Networks (RNNs), Interpretable Machine Learning

1. Introduction

In many studies, researchers face challenges in modeling and inferring from modern time-series data collected across various disciplines. Examples include healthcare (such as sleep apnea), economics (unemployment rates),

traffic and transportation (metro passenger volume), meteorology (sea surface temperature), and energy (electricity demand), among others. In these contexts, the conventional assumptions of stationarity and linearity that often form the foundation of statistical modeling are frequently inadequate. Instead, they are replaced by complex nonlinear dynamics intertwined with irregular regime shifts (Segnon et al., 2024). For instance, the unemployment rate is influenced by economic conditions like booms or recessions. It is also affected by latent continuous variables, such as regional wage elasticity, which vary with the discrete regime states. The transition of the latent variables between different steps and the interactions between the latent variables and the observations could also be nonlinear. In these settings, both conventional linear statistical models and standard deep learning approaches suffer from either severe modeling misspecification or a lack of effective identification of meaningful stochastic regimes.

Given the presence of regimes within such time series data, Switching State Space Models (switching SSMs) are arguably the most widely used. In these models, the evolution of the time series is presumed to be driven by hidden factors that switch among discrete regimes (Ghahramani and Hinton, 2000; Fox et al., 2009). The dynamics within each regime are typically represented by simple linear models that can be efficiently estimated even with a limited sample size (Durbin and Koopman, 2012), while the transitions between regimes are governed by the hidden transition probabilities of a Markov chain. For complex dependence where the stage-wise linear structure is insufficient, SSMs can be customized with certain pre-specified nonlinear transition and/or emission functions (Chow and Zhang, 2013). Despite their popularity, existing nonlinear models rely on predetermined local parametric forms with simple structures, either linear or nonlinear, which may be insufficient to describe the actual patterns in modern nonlinear time series, leading to the misspecification problem.

On the contrary, deep learning methods, especially recurrent neural networks (Hewamalage et al., 2021) with gate structures, such as the Long-Short Term Memory (LSTM, (Hochreiter and Schmidhuber, 1997)), Gated Recurrent Unit (GRU, (Chung et al., 2014)), Transformers (Chen et al., 2024; Liu et al., 2024), and temporal convolution networks (Sen et al., 2019), have emerged as the new benchmark to model nonlinear time series with highly complex dependencies. However, the classic deep learning models are deterministic and ignore the presence of unobserved stochastic signals in the dynamic system. The only randomness allowed appears in the conditional

output probability models. As deterministic models often struggle to capture stochastic behavior in nonlinear time series with non-stationary patterns and transitions (Zhang and Qi, 2005), they require a large number of parameters to ensure consistent estimation and accurate modeling. However, this is typically impractical due to the limited availability of real-world time series data in many disciplines. Additionally, deterministic deep learning models lack interpretability when applied to stochastic dynamic systems.

This has led to the integration of deep learning and stochastic latent variable models to leverage their complementary strengths of nonlinear representation and interpretability (Kingma and Welling, 2014; Rezende et al., 2014; Bayer and Osendorfer, 2014). Deep State Space Models (SSMs) often introduce continuous Gaussian latent variables at each time step to capture latent dynamics, essentially functioning as sequences of variational auto-encoders (Krishnan et al., 2017; Fraccaro et al., 2017; De Bézenac et al., 2020; Girin et al., 2021). While effective for prediction, these models struggle with interpretability in non-stationary time series due to the absence of discrete regimes. Some deep SSMs introduce discrete latent variables to model regime switching (Johnson et al., 2016; Dai et al., 2016; Liu et al., 2018). Yet, these approaches often oversimplify by assuming that time series evolution is solely driven by discrete variables, neglecting the interplay between discrete and continuous latent factors, which is crucial for capturing real-world dynamics.

We propose a Deep Switching State Space Model (DS³M) for interpretable and efficient inference in nonlinear time series with irregular regime switching. DS³M is designed to provide accurate forecasts while identifying hidden regimes with significant economic implications. The architecture combines a Recurrent Neural Network (RNN) with a Nonlinear Switching State Space Model (SSSM), where regime-switching is governed by a Markov chain. The model uses discrete latent variables to represent regimes and continuous latent variables for random driving factors, capturing the joint impact of these on the time series dynamics. Discrete latent variables influence both the observed data and continuous latent variables. The RNN enhances forecasting accuracy by leveraging long-term information and skip connections to observations. We develop an approximate variational inference algorithm that is scalable to large datasets. The key idea involves marginalizing the discrete latent variables solely at each time step and subsequently utilizing a reparametrization trick for the continuous latent variables. Applied to various domains—healthcare, economics, traffic, meteorology, and energy—DS³M outperforms state-of-the-art methods (e.g., GRU,

SRNN (Fraccaro et al., 2016), DSARF (Farnoosh et al., 2021), SNLDS (Dong et al., 2020), offering better predictive accuracy and meaningful regime identification. Notably, DS³M identifies longer regime durations, aligning more closely with real-world data compared to the chaotic switching seen in other models.

Our paper contributes a recipe for employing statistical modeling and deep learning to achieve interpretable inference for modern time series with complex dynamics. By introducing both continuous and discrete latent variables in the recurrent neural network, we efficiently harness the potent representation capabilities of continuous latent variables to capture rich dependence and enable economically meaningful identifications of discrete latent variables. The novel amortized variational inference method renders it suitable for both small and large datasets. When applied to a variety of simulated and real data across various disciplines, we showcase the robust competitive performance of DS³M compared to state-of-the-art technologies.

One of the most relevant models is the SNLDS, proposed by Dong et al. (2020). The key difference between SNLDS and our DS³M model lies in the design of both the generative model and inference algorithm. In our approach, we integrate a recurrent neural network (RNN) into DS³M to capture historical information and introduce dependencies between the observations, continuous latent variables, and the hidden states of the RNN. This enables us to address non-Markov problems within a Markov framework. The design allows the RNN and continuous latent variables to encode different types of information, leading to improved prediction accuracy, as demonstrated in our experiments. Additionally, we developed a more stable inference algorithm to mitigate posterior collapse—a situation where discrete latent variables are underutilized because the probabilistic model for continuous latent variables is overly powerful. Unlike Dong et al. (2020), where the approximate posterior of the continuous latent variables is independent of the discrete latent variables, our approach employs connected inference structures that better mimic the true posterior relationships.

The rest of the paper is organized as follows. Section 2 reviews the related works. Section 3 details the proposed DS³M and the scalable inference algorithm. Section 4 presents the numerical performance of the DS³M with several simulated and six real-world data sets in different disciplines. Section 5 concludes. Data and codes can be found on the Github website.

2. Background and related works

Denote a time series of T observations as $y_{1:T} = \{y_1, y_2, \dots, y_T\}$, $y_t \in \mathbb{R}^D$ and a sequence of inputs as $x_{1:T} = \{x_1, x_2, \dots, x_T\}$, $x_t \in \mathbb{R}^U$. In the setting of time series forecasting, x_t can be one or multiple lagged values of the time series, e.g. y_{t-1} and higher orders y_{t-2}, y_{t-3}, \dots . The inputs x_t could also contain exogenous variables. We are interested in modeling $p(y_{1:T}|x_{1:T})$.

In the class of switching SSMs, the simplest form is the switching linear dynamical system (SLDS), where the dynamics of each regime is explained by a linear state space model.

The discrete latent variables, denoted as $d_t \in \{1, 2, \dots, K\}$ at each time step $t = 1, 2, \dots, T$, follows a Markov chain. In particular, $d_t|d_{t-1}$ is assumed to follow a transition matrix $\Gamma \in \mathbb{R}^{K \times K}$, where $\Gamma_{i,j} = p(d_t = j | d_{t-1} = i)$.

The discrete latent variables d_t have impact on both the continuous latent variables $z_t \in \mathbb{R}^Z$ and y_t through the following transition and emission functions:

$$z_t = W_z^{(d_t)} z_{t-1} + W_x^{(d_t)} x_t + b_z^{(d_t)} + e_t, e_t \sim N(0, \Sigma_z^{(d_t)}) \quad (1)$$

$$y_t = W_y^{(d_t)} z_t + b_y^{(d_t)} + \epsilon_t, \epsilon_t \sim N(0, \Sigma_y^{(d_t)}) \quad (2)$$

where $W_z^{(d_t)} \in \mathbb{R}^{Z \times Z}$, $W_x^{(d_t)} \in \mathbb{R}^{Z \times U}$, $b_z^{(d_t)} \in \mathbb{R}^{Z \times 1}$, $\Sigma_z^{(d_t)} \in \mathbb{R}^{Z \times Z}$, $W_y^{(d_t)} \in \mathbb{R}^{D \times Z}$, $b_y^{(d_t)} \in \mathbb{R}^{D \times 1}$ and $\Sigma_y^{(d_t)} \in \mathbb{R}^{D \times D}$. The **transition** function in (1) determines the evolution of the latent variable. The **emission** function in (2) specifies the dynamics of the observed time series, given the state of the latent variables at time t . The transition noise e_t and emission noise ϵ_t are Gaussian distributed. When $K = 1$, the model is also termed as the Linear Gaussian State Space Model (LGSSM).

There have been several extensions to the SLDS by introducing nonlinear structures. The RSSM is proposed in Chow and Zhang (2013) which adopts a pre-specified nonlinear transition function. The SVAE model (Johnson et al., 2016) parametrizes the emission function by neural networks, while the transition function remains linear. The SNLDS model (Dong et al., 2020) parametrizes both the emission and transition functions with nonlinear neural networks. The DSARF (Farnoosh et al., 2021) approximates high-dimensional time series with a multiplication of latent factors and latent weights, where the latent weights are modeled by a nonlinear autoregressive model, switched by a Markov chain of discrete latent variables. Most of the above-mentioned work assumed that the d_t only influences the transition of

z_t . Our work, on the other hand, assumes that the d_t which represents the long-term dynamic changes of the time series, affects both y_t and z_t .

The discrete switching variables in the SLDS are assumed to be Markov, i.e. d_t depends on d_{t-1} only. The recurrent SLDS (rSLDS) proposed in Linderman et al. (2017) and Becker-Ehmck et al. (2019) extends the open-loop Markov dynamics and makes d_t depending on the hidden state z_{t-1} . In Nassar et al. (2018), a tree structure prior is imposed on the switching variables of rSLDS, where the dynamics of the switching variables behave similarly in the same subtrees. The deep Rao-Blackwellised Particle Filter proposed in Kurle et al. (2020) also allows d_t to depend on z_{t-1} . The SNLDS model (Dong et al., 2020) extends the open-loop Markov dynamics by making d_t depend on the last observations. Such recurrent structures serve as a presence of disturbance to the switching dynamics. Although such recurrent structures sometimes can improve the accuracy, they can also lead to unnecessarily frequent state shifts in the estimated discrete latent variables, making interpretations difficult, see our simulated toy example. There is a need for a well-designed architecture that allows the disturbance to be reasonably represented, and simultaneously does not lead to over frequent switching. In this work, we stick to a Markov dynamic of the discrete latent variable and push the non-Markov dynamics into the continuous latent variables that depend on the hidden states of a recurrent neural network summarizing the information coming from the past.

3. Deep Switching State Space Model (DS³M)

In this section, we will detail the generative and inference network of the DS³M.

3.1. Model

The generating model of the DS³M is as follows:

- (a) At time step t , a forward RNN is used to process the input data:

$$h_t = f_h(h_{t-1}, x_t) \tag{3}$$

where h_t is the RNN hidden state and f_h can be an LSTM or GRU.

- (b) The discrete latent variable $d_t \in \{1, \dots, K\}$ evolves following a Markov transition matrix $\Gamma \in R^{K \times K}$ with $\Gamma_{i,j} = p(d_t = j | d_{t-1} = i)$. Here K refers to the number of regime states.

- (c) The **transition function** of the continuous latent variable $z_t \in \mathbb{R}^Z$ depends on z_{t-1}, h_t, d_t and is modeled as follows:

$$z_t = \mu_{z,t}^{(d_t)} + e_t, e_t \sim N(0, \Sigma_{z,t}^{(d_t)}) \quad (4)$$

$$\mu_{z,t}^{(d_t)} = f_{z,1}^{(d_t)}(z_{t-1}, h_t), \quad \log \Sigma_{z,t}^{(d_t)} = f_{z,2}^{(d_t)}(z_{t-1}, h_t), \quad (5)$$

where the mean $\mu_{z,t}^{(d_t)} \in \mathbb{R}^Z$ and the diagonal covariance matrix $\Sigma_{z,t}^{(d_t)} = \text{Diag}(\sigma_1^{d_t}, \sigma_2^{d_t}, \dots, \sigma_Z^{d_t})$ are modeled with neural networks $f_{z,1}^{(d_t)}$ and $f_{z,2}^{(d_t)}$. In fact, $z_t \sim N(\mu_{z,t}^{(d_t)}, \Sigma_{z,t}^{(d_t)})$.

- (d) The **emission function** for the time series y_t depends on z_t, h_t, d_t and is modeled as follows:

$$y_t = \mu_{y,t}^{(d_t)} + \epsilon_t, \epsilon_t \sim N(0, \Sigma_{y,t}^{(d_t)}) \quad (6)$$

$$\mu_{y,t}^{(d_t)} = f_{y,1}^{(d_t)}(z_t, h_t), \quad \log \Sigma_{y,t}^{(d_t)} = f_{y,2}^{(d_t)}(z_t, h_t), \quad (7)$$

where the mean $\mu_{y,t}^{(d_t)} \in \mathbb{R}^D$ and the covariance matrix $\Sigma_{y,t}^{(d_t)} \in \mathbb{R}^{D \times D}$ are modeled with neural networks $f_{y,1}^{(d_t)}$ and $f_{y,2}^{(d_t)}$. In fact, $y_t \sim N(\mu_{y,t}^{(d_t)}, \Sigma_{y,t}^{(d_t)})$.

Figure 1a displays a graphical representation of the DS³M.

The DS³M differs from the SLDS model reviewed in Section 2 in several aspects: (1) DS³M introduced an RNN model to encode all the historical information in each time step. (2) The transition and the emission function become nonlinear and depend on the hidden states of the RNN.

It is also important to stress the key differences between DS³M and the state-of-the-art SNLDS. We stack an RNN below the SSSM and design a direct connection of the hidden state h_t to the time series y_t inspired by the skip connection in ResNet (He et al., 2016), Transformers (Vaswani et al., 2017) and SRNN (Fraccaro et al., 2016). While in SNLDS, there is no RNN and no hidden state h_t . Compared Equation (9) with (5), Equation (11) with (7), the transition and emission functions of the SNLDS do not depend on h_t and can be represented as

$$z_t = \mu_{z,t}^{(d_t)} + e_t, e_t \sim N(0, \Sigma_{z,t}^{(d_t)}) \quad (8)$$

$$\mu_{z,t}^{(d_t)} = f_{z,1}^{(d_t)}(z_{t-1}), \quad \log \Sigma_{z,t}^{(d_t)} = f_{z,2}^{(d_t)}(z_{t-1}), \quad (9)$$

$$y_t = \mu_{y,t}^{(d_t)} + \epsilon_t, \epsilon_t \sim N(0, \Sigma_{y,t}^{(d_t)}) \quad (10)$$

$$\mu_{y,t}^{(d_t)} = f_{y,1}^{(d_t)}(z_t), \quad \log \Sigma_{y,t}^{(d_t)} = f_{y,2}^{(d_t)}(z_t). \quad (11)$$

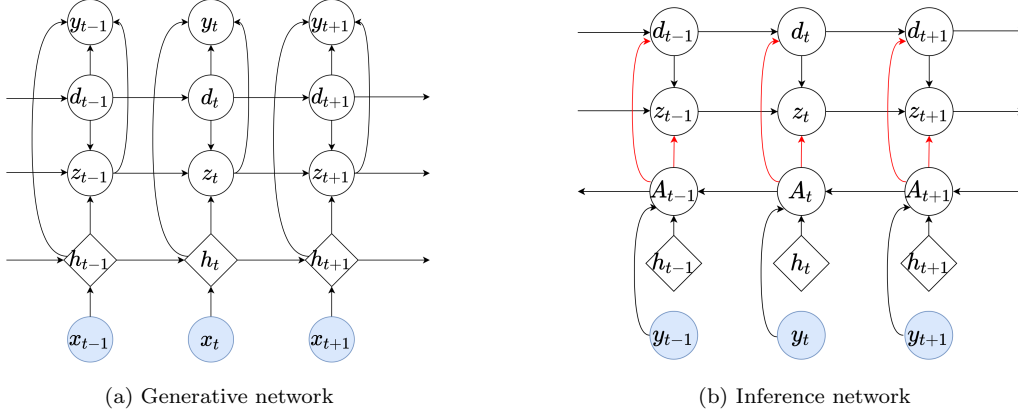


Figure 1: Deep Switching State Space Model (DS³M)

From a modeling aspect, a lack of this connection will force the continuous latent variable z_t to encode all the relevant historical information. The connection between y_t and h_t on the other hand allows a clear structure, where both the deterministic hidden states and the stochastic latent variables can separately encode different aspects of information. The addition of the RNN and the skip connection is important as we aim at the out-of-sample prediction task, while the focus of SNLDS is the segmentation of time series, i.e. identify the regimes (in-sample inference).

Remark 1. *In the emission function, we assume that the emission distribution for the time series y_t is a Gaussian distribution for simplicity. The emission distribution can be extended to other parametric distributions. For example, one could choose the emission distribution to be lognormal for asymmetric and positive time series and model the mean and variance of the lognormal distribution using neural networks.*

3.2. Estimation of parameters

Denote $\theta = \{f_h, \Gamma, \{f_{z,1}^{(k)}\}_{k=1}^K, \{f_{z,2}^{(k)}\}_{k=1}^K, \{f_{y,1}^{(k)}\}_{k=1}^K, \{f_{y,2}^{(k)}\}_{k=1}^K\}$ as the parameters of the DS³M. The joint probability is represented as

$$\begin{aligned}
 p_\theta(\mathbf{y}_{1:T}, \mathbf{z}_{1:T}, \mathbf{d}_{1:T} | \mathbf{x}_{1:T}) \\
 = \prod_{t=1}^T p_\theta(\mathbf{y}_t | \mathbf{z}_t, \mathbf{h}_t, \mathbf{d}_t) p_\theta(\mathbf{z}_t | \mathbf{z}_{t-1}, \mathbf{h}_t, \mathbf{d}_t) p_\theta(\mathbf{d}_t | \mathbf{d}_{t-1}).
 \end{aligned} \tag{12}$$

To obtain the likelihood of observations, denoted as $\mathcal{L}(\theta) = p_\theta(\mathbf{y}_{1:T} | \mathbf{x}_{1:T})$, it requires to marginal out $\mathbf{z}_{1:T}$ and $\mathbf{d}_{1:T}$ in (12). However, due to the non-linearity

introduced by neural networks, it is intractable to do the marginalization and the maximum likelihood method is not applicable for the estimation of parameters in this setting.

In order to conduct the estimation of parameters, we develop a scalable learning and inference algorithm for the DS³M using variational inference instead. Specifically, we approximate the posterior $p(\mathbf{z}_{1:T}, \mathbf{d}_{1:T} | \mathbf{x}_{1:T}, \mathbf{y}_{1:T})$ with an approximated posterior $q_\phi(\mathbf{z}_{1:T}, \mathbf{d}_{1:T} | \mathbf{y}_{1:T}, \mathbf{x}_{1:T})$ with parameter ϕ , and then maximize an evidence lower bound $\text{ELBO}(\theta, \phi) \leq \mathcal{L}(\theta)$ with respect to both θ and ϕ to obtain the parameters θ .

3.2.1. The ELBO and the approximated posterior

The $\text{ELBO}(\theta, \phi)$ can be calculated as follows:

$$\begin{aligned} \text{ELBO}(\theta, \phi) &= \mathbb{E}_{q_\phi} [\log p_\theta(\mathbf{y}_{1:T} | \mathbf{z}_{1:T}, \mathbf{d}_{1:T}, \mathbf{x}_{1:T})] \\ &\quad - \text{KL}(q_\phi(\mathbf{z}_{1:T}, \mathbf{d}_{1:T} | \mathbf{y}_{1:T}, \mathbf{x}_{1:T}) \| p_\theta(\mathbf{z}_{1:T}, \mathbf{d}_{1:T} | \mathbf{x}_{1:T})). \end{aligned} \quad (13)$$

The ELBO is tight, i.e. $\mathcal{L}(\theta) = \text{ELBO}(\theta, \phi)$, only when the approximated posterior $q_\phi(\mathbf{z}_{1:T}, \mathbf{d}_{1:T} | \mathbf{y}_{1:T}, \mathbf{x}_{1:T})$ is equal to the true posterior $p_\theta(\mathbf{z}_{1:T}, \mathbf{d}_{1:T} | \mathbf{y}_{1:T}, \mathbf{x}_{1:T})$, which is unfortunately intractable. Nevertheless, we aim to design an approximated posterior $q_\phi(\mathbf{z}_{1:T}, \mathbf{d}_{1:T} | \mathbf{y}_{1:T}, \mathbf{x}_{1:T})$ that could mimic the dynamics of the true posterior, so that we could achieve a tighter ELBO. According to the d-separation (Geiger et al., 1990) of the generative network, the true posterior can be factorized in the following form:

$$\begin{aligned} &p_\theta(\mathbf{z}_{1:T}, \mathbf{d}_{1:T} | \mathbf{y}_{1:T}, \mathbf{x}_{1:T}) \\ &= \prod_t p_\theta(\mathbf{z}_t | \mathbf{z}_{t-1}, \mathbf{d}_t, \mathbf{y}_{t:T}, \mathbf{h}_{t:T}) p_\theta(\mathbf{d}_t | \mathbf{d}_{t-1}, \mathbf{y}_{t:T}, \mathbf{h}_{t:T}), \end{aligned} \quad (14)$$

where the posterior of $\mathbf{z}_t, \mathbf{d}_t$ depends on the past information encoded in $\{\mathbf{z}_{t-1}, \mathbf{d}_{t-1}\}$ as well as the future information in $\{\mathbf{y}_{t:T}, \mathbf{h}_{t:T}\}$. Therefore, we design the approximated posterior to have the same dependency as the true posterior as follows:

$$\begin{aligned} &q_\phi(\mathbf{z}_{1:T}, \mathbf{d}_{1:T} | \mathbf{y}_{1:T}, \mathbf{x}_{1:T}) \\ &= \prod_t q_{\phi_z}(\mathbf{z}_t | \mathbf{z}_{t-1}, \mathbf{d}_t, \mathbf{A}_t) q_{\phi_d}(\mathbf{d}_t | \mathbf{d}_{t-1}, \mathbf{A}_t), \end{aligned} \quad (15)$$

where $\mathbf{A}_t = g_{\phi_A}(\mathbf{A}_{t+1}, [\mathbf{y}_t, \mathbf{h}_t])$ and $\phi = \{\phi_z, \phi_d, \phi_A\}$. We parameterize g_{ϕ_A} as a backward RNN and $q_{\phi_z}(\mathbf{z}_t | \mathbf{z}_{t-1}, \mathbf{d}_t, \mathbf{A}_t)$ with a Gaussian probabilistic density:

$$\mathbf{z}_t = \mu_{z,t}^{(d_t)} + e_t, e_t \sim N(0, 1) \quad (16)$$

$$\mu_{z,t}^{(d_t)} = g_1^{(d_t)}(z_{t-1}, \mathbf{A}_t), \quad \log \Sigma_{z,t}^{(d_t)} = g_2^{(d_t)}(z_{t-1}, \mathbf{A}_t), \quad (17)$$

where \mathbf{z}_t is a Gaussian variable with mean $\mu_{z,t}^{(d_t)}$ and diagonal variance matrix $\Sigma_{z,t}^{(d_t)}$ determined by neural network models $g_1^{(d_t)}$ and $g_2^{(d_t)}$. $z_1 \sim N(0, 1)$. Moreover, $q_{\phi_d}(\mathbf{d}_t | \mathbf{A}_t, \mathbf{d}_{t-1})$ is parameterized as a Categorical distribution:

$$d_t \sim \text{Cat}(\text{softmax}(W^{(d_{t-1})} \mathbf{A}_t)), \quad (18)$$

and $d_1 \sim \text{Uniform}(1, 2, \dots, K)$. The graphical model of the inference network is shown in Figure 1b.

3.2.2. Factorization and approximation of the ELBO

According to the conditional independence inherited in the DS³M, the conditional probability of the latent variables on the observations can be factorized in the following form:

$$p_{\theta}(\mathbf{z}_{1:T}, \mathbf{d}_{1:T} | \mathbf{x}_{1:T}) = \prod_t p_{\theta}(\mathbf{d}_t | \mathbf{d}_{t-1}) p_{\theta}(\mathbf{z}_t | \mathbf{z}_{t-1}, \mathbf{d}_t, \mathbf{h}_t). \quad (19)$$

With the approximate posterior in Equation (15) and the factorization in (19), the ELBO can be derived as follows:

$$\begin{aligned} \text{ELBO}(\theta, \phi) = \sum_t & \left\{ \mathbb{E}_{q_{\phi}^*(\mathbf{z}_{t-1}, \mathbf{d}_{t-1})} \sum_{\mathbf{d}_t} q_{\phi_d}(\mathbf{d}_t) \mathbb{E}_{q_{\phi_z}(\mathbf{z}_t)} [\log p_{\theta}(\mathbf{y}_t | \mathbf{z}_t, \mathbf{d}_t, \mathbf{h}_t)] - \right. \\ & \mathbb{E}_{q_{\phi}^*(\mathbf{z}_{t-1}, \mathbf{d}_{t-1})} \sum_{\mathbf{d}_t} q_{\phi_d}(\mathbf{d}_t) KL[q_{\phi_z}(\mathbf{z}_t | \mathbf{z}_{t-1}, \mathbf{d}_t, \mathbf{A}_t) \| p_{\theta}(\mathbf{z}_t | \mathbf{z}_{t-1}, \mathbf{d}_t, \mathbf{h}_t)] \\ & \left. - \mathbb{E}_{q_{\phi}^*(\mathbf{d}_{t-2})} \sum_{\mathbf{d}_{t-1}} q_{\phi_d}(\mathbf{d}_{t-1}) KL[q_{\phi_d}(\mathbf{d}_t | \mathbf{d}_{t-1}, \mathbf{A}_t) \| p_{\theta}(\mathbf{d}_t | \mathbf{d}_{t-1})] \right\}, \end{aligned} \quad (20)$$

where $q_{\phi}^*(\mathbf{z}_t, \mathbf{d}_t) = \int q_{\phi}(\mathbf{z}_{1:t}, \mathbf{d}_{1:t} | \mathbf{y}_{1:T}, \mathbf{x}_{1:T}) d\mathbf{z}_{1:t-1} d\mathbf{d}_{1:t-1}$ and $q_{\phi}^*(\mathbf{d}_t) = \int q_{\phi_d}(\mathbf{d}_{1:t} | \mathbf{y}_{1:T}, \mathbf{x}_{1:T}) d\mathbf{d}_{1:t-1}$. The detailed derivation can be found in Appendix A.

We can approximate the ELBO in (20) using a Monte Carlo method. We need to obtain samples $(z_t^{(s)}, d_t^{(s)})$ for $t = 1 \dots, T$ from $q_{\phi}^*(\mathbf{z}_t, \mathbf{d}_t)$ using ancestral sampling according to Equation (15). Given a sample $(\mathbf{z}_{t-1}^{(s)}, \mathbf{d}_{t-1}^{(s)})$ from $q_{\phi}^*(\mathbf{z}_{t-1}, \mathbf{d}_{t-1})$, a sample $(\mathbf{z}_t^{(s)}, \mathbf{d}_t^{(s)})$ from $q_{\phi}(\mathbf{z}_t, \mathbf{d}_t | \mathbf{z}_{t-1}^{(s)}, \mathbf{d}_{t-1}^{(s)}, \mathbf{y}_{t:T}, \mathbf{h}_{t:T})$ will follow $q_{\phi}^*(\mathbf{z}_t, \mathbf{d}_t)$. Therefore, we could adopt the following procedures to obtain the Monte Carlo samples $(z_t^{(s)}, d_t^{(s)})$ for $t = 1 \dots, T$:

- i. Sample $d_1^{(s)} \sim \text{Uniform}(1, 2, \dots, K)$, sample $z_1^{(s)} \sim N(0, 1)$
- ii. For $t = 2, \dots, T$, sample $d_t^{(s)}$ according to the density $q_{\phi_d}(\mathbf{d}_t | \mathbf{A}_t, \mathbf{d}_{t-1})$ based on Equation (18); sample $z_t^{(s)}$ according to the density $q_{\phi_z}(\mathbf{z}_t | \mathbf{z}_{t-1}, \mathbf{d}_t, \mathbf{A}_t)$ based on Equation (16) and (17).

The approximated ELBO can then be represented as follows:

$$\begin{aligned} \text{ELBO}(\theta, \phi) \approx \sum_t \bigg\{ & \sum_{\mathbf{d}_t} q_{\phi_d}(\mathbf{d}_t) \log p_{\theta}(\mathbf{y}_t | \mathbf{z}_t^{(s)}, \mathbf{d}_t, \mathbf{h}_t) \\ & - \sum_{\mathbf{d}_t} q_{\phi_d}(\mathbf{d}_t) KL \left[q_{\phi_z}(\mathbf{z}_t | \mathbf{z}_{t-1}^{(s)}, \mathbf{d}_t, \mathbf{A}_t) \parallel p_{\theta}(\mathbf{z}_t | \mathbf{z}_{t-1}^{(s)}, \mathbf{d}_t, \mathbf{h}_t) \right] \\ & - \sum_{\mathbf{d}_{t-1}} q_{\phi_d}(\mathbf{d}_{t-1}) KL [q_{\phi_d}(\mathbf{d}_t | \mathbf{d}_{t-1}, \mathbf{A}_t) \parallel p_{\theta}(\mathbf{d}_t | \mathbf{d}_{t-1})] \bigg\}. \end{aligned} \quad (21)$$

3.2.3. Gradients of the ELBO

We use the gradient descent algorithm to optimize the approximated ELBO in (21). While it is easy to obtain the gradient of ELBO with respect to θ ($\nabla_{\theta} \text{ELBO}(\theta, \phi)$), it is not the case for the gradient of ELBO with respect to ϕ ($\nabla_{\phi} \text{ELBO}(\theta, \phi)$). The score function gradient estimator (Williams, 1992) suffers from high variance and the reparameterization approach is often used to reduce the variance (Rezende et al., 2014; Kingma and Welling, 2014).

For the continuous latent variable z_t in the ELBO, we apply the reparameterization approach. Specifically, we generate a sample $e_t \sim N(0, 1)$, and then use $\mu_t + \epsilon_t \Sigma_t$ as a sample of $z_t \sim N(\mu_t, \Sigma_t)$ in the above Monte Carlo approximation. By adopting this approach, the gradients can then be backpropagated through the continuous random variables.

The reparameterization trick, however, is not applicable for the discrete random variable d_t . One commonly used reparameterization trick for discrete random variables is the Gumbel-softmax reparameterization trick (Dong et al., 2020). However, this will result in non-interger sampling values for d_t , which are invalid for our model. As an alternative approach, in (21), we marginalize out the discrete variable d_t with a summation over its probability at each time step t , and do not marginalize out the discrete variable before time t . This introduces a biased gradient estimator for ϕ_d and ϕ_z and it can be viewed as gradient clips where the gradients from the previous time steps are ignored. In our experiments, such an approximation performs very well compared to the unbiased score function estimator and we consider the bias negligible. We have done some experiments that marginalized more than one step in (21). The performance is similar, but the time complexity in computing (21) will increase from $O(KT)$ to $O(K^2T)$. Therefore, we stick to the current setting.

It is worth mentioning that the SNLDS marginalizes the discrete latent variables using the exact posterior derived with the forward-backward algorithm, while the DS³M marginalizes the discrete latent variables using the approximate posterior at each time step. One potential problem of marginalizing the discrete latent variables using the exact posterior is that the approximate posterior for z_t does not depend on d_t anymore. This could lead to a severe posterior collapse problem that d_t is not used at all. They proposed an entropy regularizer to encourage an evenly distributed posterior for d_t . However, there is no guarantee that an evenly distributed posterior will produce a meaningful interpretation. In contrast, we use an approximated posterior of z_t that depends on d_t to form a connected inference between z_t and d_t . The posterior collapse problem for the discrete latent variables does not appear in our experiments.

A summary of the structured inference algorithm is given in Algorithm 1.

Algorithm 1 Structured Inference Algorithm for DS³M

Inputs: $\{x_{1:T}\}_{i=1}^N$, $\{y_{1:T}\}_{i=1}^N$, randomly initialized $\phi^{(0)}$ and $\theta^{(0)}$

Outputs: θ , ϕ

while $Iter < M$ **do**

1. Sample a mini-batch sequences $\{x_{1:T}\}_{i=1}^B$, $\{y_{1:T}\}_{i=1}^B$ from the dataset
2. Generate $z_t^{(s)}, d_t^{(s)}$ for $t = 1, 2, \dots, T$ sequentially according to (15) to approximate the ELBO in (21)
3. Derive $\nabla_{\theta} \text{ELBO}(\theta, \phi)$ and $\nabla_{\phi} \text{ELBO}(\theta, \phi)$
4. Update $\theta^{(Iter)}, \phi^{(Iter)}$ using the ADAM, set $Iter = Iter + 1$

end while

Remark 2. *In our paper, we assume the number of switching statuses to be known. It is possible to use a Bayesian mixture modeling approach (Giudici et al., 2003) to automatically determine the number of switch statuses in our DS³M model. However, adapting our model to this non-parametric Bayesian framework is not trivial. It would require joint modeling of the number of switch statuses along with the parameters of the DS³M, as well as a redesign of the estimation algorithm of the parameters. Therefore, we leave this for future research.*

Both underestimation and overestimation of the number of switching statuses can lead to suboptimal forecasting performance. Specifically, underestimating the regimes may result in modeling bias and reduced adaptability to

regime shifts, while overestimating can increase the variance in predictions due to overfitting, thereby reducing the robustness of forecasts.

To mitigate this issue, we suggest employing data-driven methods, such as cross-validation, to select the optimal number of states. Additionally, extending likelihood-based tests (Giudici et al., 2000) to this context could be another viable approach. We consider this a direction for future research.

3.3. Predictive distributions

Given a trained model, we are interested in the predictive distributions for the one-step-ahead to τ -step-ahead observations $\{y_{T+1}, \dots, y_{T+\tau}\}$ and the discrete latent variables $\{d_{T+1}, \dots, d_{T+\tau}\}$. We first make inference on the posterior distributions of $\{z_t, d_t\}_{t=1}^T$ and then generate samples of $\{z_t^{(s)}, d_t^{(s)}, y_t^{(s)}\}_{t=T}^{T+\tau}$, $s = 1, \dots, S$ and S represents the number of Monte Carlo samples. The predictive distributions are then approximated with the empirical distribution functions of the generated samples. The predictive distributions can be obtained as follows:

$$\begin{aligned} p(y_{T+1}|x_{1:T}, y_{1:T}) &\approx \frac{1}{S} \sum_{s=1}^S p(y_{T+1}|z_{T+1}^{(s)}, h_{T+1}), \\ p(d_{T+1}|x_{1:T}, y_{1:T}) &\approx \frac{1}{S} \sum_{s=1}^S p(d_{T+1}|d_T^{(s)}), \\ p(z_{T+1}|x_{1:T}, y_{1:T}) &\approx \frac{1}{S} \sum_{s=1}^S p(z_{T+1}|d_{T+1}^{(s)}, z_T^{(s)}). \end{aligned} \quad (22)$$

3.4. Theoretical analysis of the DS³M

In the following, we demonstrate the presence of stability of DS³M.

The latent continuous state in DS³M $z_t \sim \mathcal{N}(\mu_{z,t}^{(d_t)}, \Sigma_{z,t}^{(d_t)})$ where the mean $\mu_{z,t}^{(d_t)}$ and the diagonal covariance matrix $\Sigma_{z,t}^{(d_t)}$ are parameterized by neural networks $f_{z,1}^{(d_t)}$ and $f_{z,2}^{(d_t)}$, respectively. Similarly, the observed time series is modeled as $y_t \sim \mathcal{N}(\mu_{y,t}^{(d_t)}, \Sigma_{y,t}^{(d_t)})$, where the mean $\mu_{y,t}^{(d_t)}$ and the covariance matrix $\Sigma_{y,t}^{(d_t)}$ are parameterized by neural networks $f_{y,1}^{(d_t)}$ and $f_{y,2}^{(d_t)}$, respectively.

Theorem 1. *The DS³M is stable, i.e. the latent variable z_t and the observed variable y_t are globally mean-square stable if the 2-norms of all weight matrices and activation scaling matrices are upper bounded by 1.*

Since DS³M employs ReLU (Rectified Linear Unit) activation functions, this naturally satisfies the constraints on activation scaling matrices. Global mean-square stability guarantees that the system states remain bounded in

the mean-square sense over time, effectively preventing divergence and ensuring the reliability of long-term predictions. This property enhances the robustness and generalization capabilities of DS³M, making it a reliable framework for capturing intricate temporal dependencies and ensuring consistent performance across diverse datasets. The proof for the Theorem 1 is provided in the Appendix.

4. Experiments

In this section, we evaluate DS³M through various experiments. We first consider a simulated 1-dimensional (1-d) time series whose true dynamics follow a nonlinear switching state space model, as well as a simulated 10-dimensional (10-d) time series based on the Lorenz attractor. Furthermore, we apply DS³M to several real-world datasets spanning diverse applications, such as health care, transportation, energy, and econometrics. Both simulations and real data analyses demonstrate that DS³M effectively captures switching regimes and achieves competitive predictive accuracy when compared with several state-of-the-art methods, including SRNN, GRU, DSARF, and SNLDS. Specifically, SRNN can be considered our model without discrete latent variables. DSARF and SNLDS are two nonlinear dynamic latent variable models for time series that incorporate both continuous and discrete latent variables. DSARF’s superior performance over models like rSLDS and SLDS in time series forecasting with similar datasets has been demonstrated (Farnoosh et al., 2021). Hence, we omit the comparison of SLDS and rSLDS in the subsequent analysis. To ensure a fair comparison, we select the same datasets and employ the official codes of DSARF and SNLDS. Further details about hyperparameters are provided in the supplementary material. For a fair comparison, we select the same data sets and use the official codes of DSARF and SNLDS. Details of the hyperparameters are provided in the supplementary material.

4.1. Simulations

Toy example. For the toy simulated example, we simulated data with a length of 2000 from the following nonlinear switching state space model:

$$\begin{aligned}
d_0 &\sim \text{Bernouli}(0.5), z_0 = 0 \\
d_t|d_{t-1} &\sim \Gamma = \begin{bmatrix} 0.95 & 0.05 \\ 0.05 & 0.95 \end{bmatrix}, d_t \in \{0, 1\} \\
Z_{t|d_t=0} &= 0.6Z_{t-1} + 0.4 \times \tanh(X_t + Z_{t-1}) + w_t^{(0)}, \\
Z_{t|d_t=1} &= 0.1Z_{t-1} + 0.2 \times \sin(X_t + Z_{t-1}) + w_t^{(1)}, \\
Y_{t|d_t=0} &= 1.5Z_t + \tanh(Z_t) + v_t^{(0)}, \\
Y_{t|d_t=1} &= 0.5Z_t + \sin(Z_t) + v_t^{(1)}, \\
w_t^{(0)} &\sim N(0, 10), w_t^{(1)} \sim N(0, 1), \\
v_t^{(0)} &\sim N(0, 5), v_t^{(1)} \sim N(0, 0.5)
\end{aligned} \tag{23}$$

For the simulated time series, the switching indicator d_t controls both the dynamics of the continuous latent variable z_t and the observation y_t . By design, y_t is much more volatile (has higher variance) when $d_t = 0$ compared with $d_t = 1$. Note that we crafted the Markovian transition matrix with the intention of maintaining a high probability for the regime to remain in its current state, rather than undergoing frequent and chaotic shifts. This deliberate design choice reflects the characteristics often observed in various real-world contexts. Our aim is to closely mimic the realistic settings of these fields, where the relative stability of regimes is a prevalent feature. We transform the time series into subsequences with a length of 20, resulting in 1980 subsequences. The first 1000, the following 480, and the last 500 subsequences are used for training, validation, and testing. We set $x_t = y_{t-1}$.

Figure 2a showcases the one-step-ahead forecasting results (one experiment run) of DS³M for the testing data, along with the predicted switching indicators of DS³M, SNLDS, and DSARF. Notably, the predictive means of the observations closely align with the actual observations, while the 90% confidence intervals effectively encompass a majority of the data points. Furthermore, DS³M adeptly adapts by offering wider confidence intervals during volatile periods and narrower ones during more stable data phases. Importantly, the learned transition matrix, $\begin{bmatrix} 0.91 & 0.09 \\ 0.18 & 0.82 \end{bmatrix}$, exhibits close alignment with the true transition matrix.

Table 1: Summary of the simulation results (mean \pm standard deviation) over five experiment runs

		Toy			Lorenz		
		DS ³ M	SNLDS	DSARF	DS ³ M	SNLDS	DSARF
Forecasting	RMSE	14.572 \pm 0.352	16.541 \pm 0.024	15.244 \pm 0.136	0.168 \pm 0.017	0.226 \pm 0.065	0.030 \pm 0.000
	Duration for dt=1	7.509 \pm 1.579	1.282 \pm 0.001	3.946 \pm 0.426	-	-	-
	Duration for dt=0	7.634 \pm 1.667	1.667 \pm 0.012	3.274 \pm 0.985	-	-	-
	Accuracy (%)	0.788 \pm 0.033	0.543 \pm 0.001	0.765 \pm 0.047	0.882 \pm 0.079	0.616 \pm 0.065	0.788 \pm 0.143
	F1 score	0.778 \pm 0.023	0.549 \pm 0.001	0.757 \pm 0.035	0.837 \pm 0.127	0.600 \pm 0.100	0.775 \pm 0.124
Inference	Accuracy (%)	0.849 \pm 0.004	0.692 \pm 0.003	0.819 \pm 0.044	0.911 \pm 0.068	0.744 \pm 0.174	0.789 \pm 0.146
	F1 score	0.831 \pm 0.005	0.544 \pm 0.002	0.808 \pm 0.039	0.883 \pm 0.103	0.680 \pm 0.244	0.761 \pm 0.113

Table 1 presents a summary of forecasting and inference accuracy across five experiment runs. DS³M excels with lower forecasting RMSE (Root Mean Square Error) for observations, showing a relative enhancement of 11.46% and 4.41% over SNLDS and DSARF respectively. Furthermore, DS³M achieves significantly higher state prediction accuracy (with a relative improvement of 44.99% compared to SNLDS) and a higher F1 score (with a relative improvement of 41.77% compared to SNLDS) for the switching indicators. While DSARF and DS³M exhibit comparable state prediction accuracy and F1 score, Figure 2a shows that DS³M provides much more reliable predictions for switching indicators as compared to the ground truth, while SNLDS and DSARF tend to switch too frequently. The mean duration lengths of the two states in DS³M are 7.509 and 7.634, although they are still smaller than the true values (24 and 24). However, this performance is notably better than the alternatives, where duration lengths range around 1–4. When applied to segmenting time series (inference), DS³M also showcases superior accuracy and F1 scores compared to SNLDS, while performing similarly to DSARF.

Lorenz attractor. Lorenz attractor is a canonical nonlinear dynamical system with the following nonlinear dynamic for $z_t = [z_{t,1}, z_{t,2}, z_{t,3}]$:

$$\frac{dz}{dt} = \begin{bmatrix} \alpha(z_2 - z_1) \\ z_1(\beta - z_1) - z_2 \\ z_1 z_2 - \gamma z_3 \end{bmatrix} \quad (24)$$

The variable $z_t = [z_{t,1}, z_{t,2}, z_{t,3}]^T$ is treated as a latent variable and thus is unobservable. In the simulation, we considered a 10-dimensional time series $y_t = Wz_t + v_t$, where $W \in R^{10 \times 3}$, $v_t \sim N(0, 0.5I_{10})$. The same dataset was used in Farnoosh et al. (2021). Similar to the toy example, we set $x_t = y_{t-1}$.

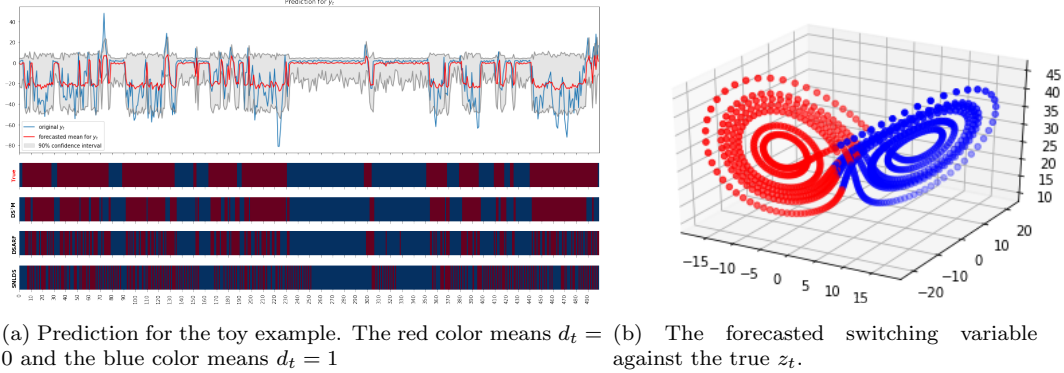


Figure 2: Plots for the two simulated datasets

The traces of the Lorenz attractor can be roughly separated into two ellipses. We simulated a time series with a length of 3000 and transformed the time series into subsequences with a length of 5, resulting in 2990 subsequences. The first 1000, the following 990, and the last 1000 subsequences are used for training, validation, and testing respectively.

The forecasted switching variables of the DS³M are shown in Figure 2b. The model successfully separates the two ellipses with a forecasting accuracy of 0.882 ± 0.079 (a relative improvement of 43.14% and 11.99% compared with SNLDS and DSARF respectively) and an F1 score of 0.837 ± 0.127 (a relative improvement of 39.50% and 8.11%), see Table 1. For the forecasting accuracy of the observations, the DS³M has smaller RMSE and MAPE compared to SNLDS, but did not beat DSARF. The superior performance of the DSARF is because the simulated dataset is generated as a multiplication of weights and factors, which fits the assumption of the generative model of the DSARF. As for the segmentation task (inference), the DS³M also achieves the highest accuracy: 0.911 ± 0.068 (a relative improvement of 22.51% and 15.49%) and best F1 score: 0.883 ± 0.103 (a relative improvement of 29.97% and 16.06%).

We conducted additional experiments by setting the number of switching states to 3 for this simulated dataset. The results show that it succeeds in learning to only use two states and ignore the redundant state. The redundant state has a very small average predictive probability (0.073) over the test samples, while for the other two states, the average predictive probability is 0.512 and 0.414 respectively.

4.2. Real data analysis

We conducted a thorough evaluation of DS³M’s performance across six real-world datasets, encompassing diverse fields. These datasets are: **Sleep** Apnea, the US **unemployment** rate, **Hangzhou** metro, **Seattle** traffic and **Pacific** surface temperature, and French **electricity** demand. These datasets not only span a range of disciplines but also exhibit varying data characteristics in terms of sampling frequency and dimensionality. Here is a brief overview of each dataset:

- the **Sleep** Apnea dataset is a public physiological dataset from a patient diagnosed with sleep apnea, a medical condition in which patients intermittently stop breathing during sleep. The respiration pattern in sleep apnea can be characterized by at least two regimes – no breathing and gasping breathing induced by reflex arousal. We use the same separation of training and testing data as in Ghahramani and Hinton (2000) and Farnoosh et al. (2021).
- The monthly US **Unemployment** rate¹ is one of the most important indicators of the US economy. The data are from January 1948 to March 2021 and the last 20 years are used for testing.
- The **Hangzhou** Metro dataset ² consists of the incoming passenger flow of 80 metro stations in Hangzhou, China from January 1 to January 25, 2019 (Farnoosh et al., 2021). The passenger flow data have a temporal resolution of 10-minutes during the service hour, i.e. 108 points per day. The last 5 days are used for testing.
- The **Seattle** Traffic dataset³ contains the traffic speed from 323 loop detectors in Seattle, USA, from January 1 to January 28, 2015 (Farnoosh et al., 2021). It has a temporal resolution of 5-min, i.e. 288 points in a day. The last 5 days are reserved for testing.

¹US Unemployment Rate, <https://fred.stlouisfed.org/series/UNRATE>

²Hangzhou Incoming Passenger Flow, <https://tianchi.aliyun.com/competition/entrance/231708/>

³Seattle Inductive Loop Detector Dataset, <https://github.com/zhiyongc/Seattle-Loop-Data>

- The **Pacific** surface temperature dataset⁴ consists of monthly surface temperatures of the Pacific for 2520 gridded spatial locations from January 1970 to December 2002 (Farnoosh et al., 2021). The last 5 years are used for testing.
- The French **Electricity** demand dataset contains half-hourly electricity demand in France from January 1, 2012 to December 31, 2019, which is also used in Xu et al. (2021); Cho et al. (2013). The year 2019 is used for testing. For this dataset, we only have one time series, and the testing data spans one year.

A summary of the data sets is provided in Table 2 and more details are given in the supplementary materials. We performed both short-term and long-term forecasting. For short-term prediction, we conducted one-step ahead forecasting with rolling windows. All models were trained for 100 epochs on the data preceding the test data and remained fixed during the forecasting of the test data. For long-term prediction, we performed forecasting for the entire test data sequentially, starting from the beginning of the test dataset.

Table 2: Description of the datasets

Dataset	frequency	D	$T+T_{\text{test}}$	T_{test}
Sleep	half a second	1	2000	1000 (500 seconds)
Unemployment	month	1	879	240 (20 years)
Hangzhou	10 mins	80	2700	540 (5 days)
Seattle	5 mins	323	8064	1440 (5 days)
Pacific	month	2520	396	60 (5 years)
Electricity	half a hour	48	2921	320 days (1 year)

Short-term prediction results. Table 3 presents the prediction results for the six datasets in terms of both MAPE (Mean Absolute Percentage Error) and RMSE (Root Mean Square Error), as defined in the supplementary materials. DS³M demonstrates superior performance across the board. Specifically, for the Sleep, Unemployment rate, Seattle, and Electricity datasets, DS³M outperforms all alternative models in terms of both RMSE and MAPE. Notably, the RMSE values exhibit relative improvements ranging from 5.0%-56.9%, 28.9%-62.8%, 0.5%-6.3%, and 18.4%-66.3% for these four datasets, while the MAPE values demonstrate reductions of 15.71%-72.60%, 0.60%-18.62%, 0.09%-1.46%, and 0.76%-14.06% against the alternative models. For the

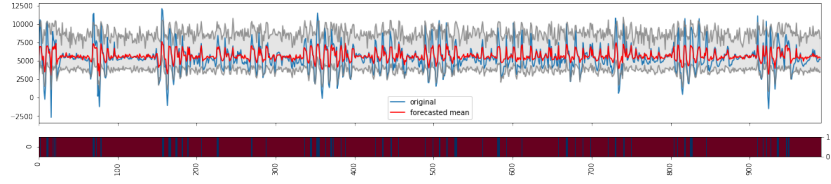
⁴Pacific Ocean Temperature Dataset, <http://iridl.ldeo.columbia.edu/>

Table 3: Comparison of RMSE and MAPE on testing data. The best models are in bold. “-” indicates the model forecasts diverge to unreasonable values and are omitted.

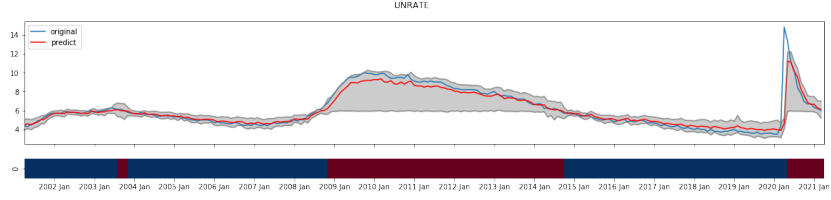
	Datasets	RMSE					MAPE (%)				
		DS ³ M	SNLDS	DSARF	SRNN	GRU	DS ³ M	SNLDS	DSARF	SRNN	GRU
Short-term	Sleep	1201	2789	1557	1806	<u>1264</u>	15.46	88.06	39.25	50.8	<u>31.17</u>
	Unemployment	0.75	1.59	1.06	2.01	<u>1.05</u>	4.53	16.13	8.11	23.15	<u>5.13</u>
	Hangzhou	32.53	36.67	34.81	<u>33.80</u>	38.42	<u>24.04</u>	23.90	29.73	25.40	30.48
	Seattle	4.16	4.18	4.44	<u>4.17</u>	4.18	5.81	<u>5.85</u>	7.27	6.00	6.89
	Pacific	0.57	15.78	0.53	0.58	<u>0.56</u>	1.69	58.01	1.57	1.74	<u>1.68</u>
	Electricity	2971	5133	8805	<u>3642</u>	4784	4.58	7.79	18.64	<u>5.34</u>	6.60
Long-term	Hangzhou	47.50	<u>42.83</u>	42.28	60.89	73.18	38.20	50.6	<u>43.65</u>	82.81	86.61
	Seattle	4.17	4.19	-	4.17	16.93	5.81	5.86	-	5.81	27.95
	Pacific	0.72	-	<u>0.73</u>	0.98	0.76	2.15	-	2.29	2.99	2.22

Hangzhou dataset, DS³M achieves the lowest RMSE and exhibits comparable MAPE to SNLDS (the best-performing model for this dataset). For the Pacific dataset, DS³M attains competitive performance comparable to DSARF, which holds the best performance in this context. We also conducted the DM test (Diebold and Mariano, 2002) to check whether the forecast errors from the models are significantly different. The test confirms that the DS³M model significantly outperforms the alternatives for the Sleep, Unemployment rate, and Electricity datasets according to the DM test. There is no significant difference between the DS³M and the best alternatives for the Seattle, Hangzhou, and Pacific datasets.

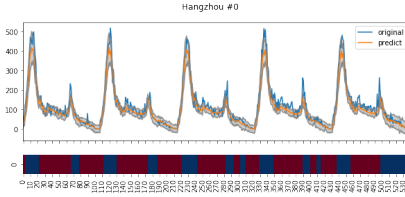
Figure 3 visually presents the short-term predictions of the testing data along with the identified switching regimes for various datasets. For the **Sleep** dataset, DS³M segregates the time series into two distinct regimes represented by blue and red shades. Notably, the consistent red regime is found to correspond to periods when the patient experiences little to no breathing, while the blue regime corresponds to periods marked by gasping breaths. In the case of **Unemployment** rates, DS³M successfully separates the time series into two regimes. The red regimes align with times of elevated unemployment, notably during the 2009 financial crisis and the 2020 Covid-19 pandemic. Further, specific illustrations showcase values at randomly selected locations for datasets such as Hangzhou, Seattle, Pacific, and French Electricity demand. DS³M’s automated segmentation of Hangzhou traffic data into peak and non-peak hours is particularly noteworthy. In the context of the **Seattle** dataset, the red regime signifies periods of heightened traffic volatility. In the **Pacific** dataset, different regimes are associated with shifts in the time series level. For instance, at Location 0, the red regime exhibits a higher level compared to the blue regime, while the reverse is true



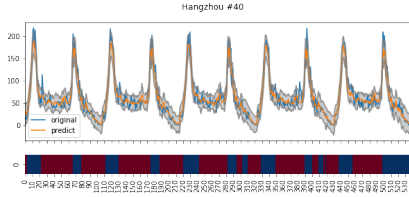
(a) Sleep apnea (measured at 2 Hz)



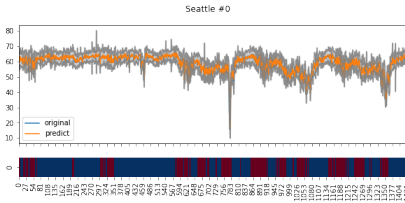
(b) US unemployment rate



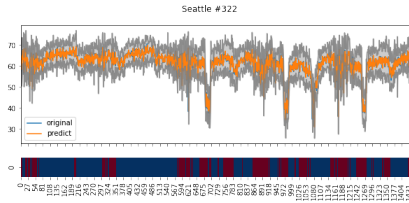
(c) Hangzhou metro station 0



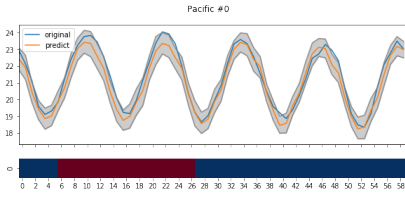
(d) Hangzhou metro station 40



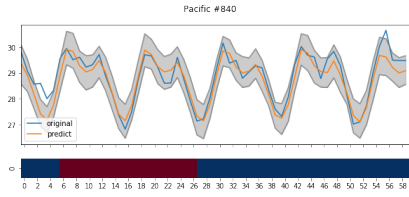
(e) Seattle traffic loop 0



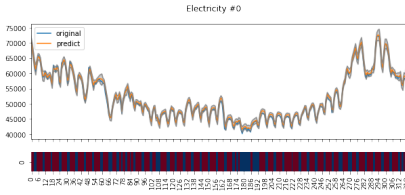
(f) Seattle traffic loop 322



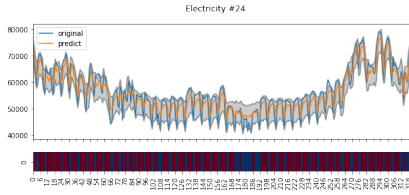
(g) Pacific location 0



(h) Pacific location 840



(i) French Electricity 0:00



(j) French Electricity 12:00

Figure 3: Predictions of the testing data for different datasets

for Location 840. Lastly, for the French **Electricity** demand dataset, the red regime is found to align predominantly with working days, while the blue regime corresponds to weekends. In general, it shows that all the predicted values trace the true values closely and the 90% confidence intervals cover most of the true values in the future. It is worth noting that unlike models that involve multiple features and use metrics such as Shapley values for feature importance (Babaei et al., 2025), DS³M focuses on interpreting latent regimes only using lagged values of the time series. Its main contribution lies in the ability to precisely identify latent regimes, providing insights into changes in dynamic behavior. This interpretability centers on understanding the dynamics and changes in latent regimes over time. By modeling the switching behavior and capturing transitions between different regimes, DS³M is able to provide insights into the underlying processes driving the data and provide economic interpretation, in addition to the enhanced forecast accuracy.

Long-term prediction results. In the long-term prediction experiment, we excluded the Sleep and Unemployment datasets due to their lack of periodic patterns and high chaotic nature, making them unsuitable for long-term prediction assessment. Similarly, the Electricity dataset was omitted from the long-term prediction analysis, given its test length spanning one year, which renders long-term predictions less practical for high-frequency data across all models.

Table 3 showcases the long-term forecasting errors for the various datasets. Notably, DS³M exhibits superior performance in terms of RMSE for the Pacific dataset. For both Hangzhou and Pacific datasets, DS³M outperforms the alternatives in terms of MAPE. Regarding the Seattle dataset, DS³M and SRNN demonstrate comparable performance. These findings highlight DS³M’s favorable outcomes in the context of long-term predictions, especially for the specific datasets mentioned. The DM test shows that the DS³M model significantly outperforms the best alternatives for the Pacific dataset, while there is no significant difference for the Seattle dataset. For the Hangzhou dataset, DSARF slightly outperforms DS³M, but in terms of MAPE, DS³M performs better.

These results indicate that although DS³M is not consistently the best model, it is often the best or second-best model. The performance of DS³M is generally more robust compared to the alternatives.

5. Conclusion

We proposed the deep switching state space model (DS³M) for forecasting nonlinear time series characterized by regime switching. DS³M effectively captures these intricate dynamics by utilizing both discrete and continuous latent variables in conjunction with recurrent neural networks. This distinctive approach combines the power of deep learning with stochastic latent variable models, enabling accurate and interpretable forecasting.

A key strength of DS³M lies in its versatility across diverse datasets. The model’s architecture, comprised of a recurrent neural network (RNN) and a nonlinear switching state space model (SSSM), is capable of accommodating small and large data alike. The amortized variational inference method, employed for estimation, trains both the inference and generative networks together, ensuring applicability across varying data scales. The DS³M’s efficacy is demonstrated across a range of simulated and real-world datasets, showcasing its competitive performance relative to several state-of-the-art methods.

There are some limitations of the proposed model. Firstly, an open loop of the transition of the discrete variable is not considered, as we found during the experiments that the current open-loop design by making the discrete latent variables always depend on the continuous latent variables and/or observations may lead to unnecessarily frequent switching of the latent variables. If there is a time series with ultra-frequent regime switching behaviors, such a recurrent structure may be useful. More sophisticated architecture can be designed to account for this and we leave it for future research. Secondly, it is challenging to choose the number of switching states. This is an open question in the literature. Future work can use a Dirichlet prior to automatically deciding the number of switching states.

These contributions establish DS³M as a robust and adaptable tool for forecasting complex nonlinear time series, offering a bridge between the worlds of deep learning and latent variable models. As this field evolves, DS³M is positioned to enhance our ability to model and understand intricate dynamics in diverse applications.

Acknowledgments

We acknowledge the financial support provided by grants A-8000828-00-00 and A-8000828-01-00 (Regime-Switching Markov Decision Process with

Applications in Digital FinTech), as well as grant A-8000014-00-00 (Deep State Space Models for Non-stationary Time Series).

References

- M. Segnon, R. Gupta, B. Wilfling, Forecasting stock market volatility with regime-switching garch-midas: The role of geopolitical risks, *International Journal of Forecasting* 40 (2024) 29–43.
- Z. Ghahramani, G. E. Hinton, Variational learning for switching state-space models, *Neural Computation* 12 (2000) 831–864.
- E. Fox, E. B. Sudderth, M. I. Jordan, A. S. Willsky, Nonparametric bayesian learning of switching linear dynamical systems, in: *Advances in Neural Information Processing Systems*, 2009, pp. 457–464.
- J. Durbin, S. J. Koopman, *Time series analysis by state space methods*, volume 38, Oxford University Press, 2012.
- S.-M. Chow, G. Zhang, Nonlinear regime-switching state-space (RSSS) models, *Psychometrika* 78 (2013) 740–768.
- H. Hewamalage, C. Bergmeir, K. Bandara, Recurrent neural networks for time series forecasting: Current status and future directions, *International Journal of Forecasting* 37 (2021) 388–427.
- S. Hochreiter, J. Schmidhuber, Long short-term memory, *Neural Computation* 9 (1997) 1735–1780.
- J. Chung, C. Gulcehre, K. Cho, Y. Bengio, Empirical evaluation of gated recurrent neural networks on sequence modeling, in: *NIPS 2014 Workshop on Deep Learning*, 2014, pp. 1–9.
- Y. Chen, K. Ren, Y. Wang, Y. Fang, W. Sun, D. Li, Contiformer: Continuous-time transformer for irregular time series modeling, *Advances in Neural Information Processing Systems* 36 (2024).
- Y. Liu, T. Hu, H. Zhang, H. Wu, S. Wang, L. Ma, M. Long, itransformer: Inverted transformers are effective for time series forecasting, in: *The Twelfth International Conference on Learning Representations*, 2024. URL: <https://openreview.net/forum?id=JePfAI8fah>.

- R. Sen, H.-F. Yu, I. S. Dhillon, Think globally, act locally: A deep neural network approach to high-dimensional time series forecasting, in: *Advances in Neural Information Processing Systems*, 2019, pp. 4837–4846.
- G. P. Zhang, M. Qi, Neural network forecasting for seasonal and trend time series, *European Journal of Operational Research* 160 (2005) 501–514.
- D. P. Kingma, M. Welling, Auto-encoding variational bayes, in: *International Conference on Learning Representations*, 2014, pp. 1–9.
- D. J. Rezende, S. Mohamed, D. Wierstra, Stochastic backpropagation and approximate inference in deep generative models, in: *International Conference on Machine Learning*, 2014, pp. 1278–1286.
- J. Bayer, C. Osendorfer, Learning stochastic recurrent networks, in: *NIPS 2014 Workshop on Advances in Variational Inference*, 2014, pp. 1–9.
- R. G. Krishnan, U. Shalit, D. Sontag, Structured inference networks for nonlinear state space models., in: *Proceedings of the AAAI Conference on Artificial Intelligence*, 2017, pp. 2101–2109.
- M. Fraccaro, S. Kamronn, U. Paquet, O. Winther, A disentangled recognition and nonlinear dynamics model for unsupervised learning, in: *Advances in Neural Information Processing Systems*, 2017, pp. 3601–3610.
- E. De Bézenac, S. S. Rangapuram, K. Benidis, M. Bohlke-Schneider, R. Kurl, L. Stella, H. Hasson, P. Gallinari, T. Januschowski, Normalizing kalman filters for multivariate time series analysis, in: *Advances in Neural Information Processing Systems*, 2020, pp. 2995–3007.
- L. Girin, S. Leglaive, X. Bie, J. Diard, T. Hueber, X. Alameda-Pineda, Dynamical variational autoencoders: A comprehensive review, *Foundations and Trends in Machine Learning* 15 (2021) 1–175.
- M. Johnson, D. K. Duvenaud, A. Wiltchko, R. P. Adams, S. R. Datta, Composing graphical models with neural networks for structured representations and fast inference, in: *Advances in Neural Information Processing Systems*, 2016, pp. 2946–2954.
- H. Dai, B. Dai, Y.-M. Zhang, S. Li, L. Song, Recurrent hidden semi-markov model, in: *International Conference on Learning Representations*, 2016, pp. 1–17.

- H. Liu, L. He, H. Bai, B. Dai, K. Bai, Z. Xu, Structured inference for recurrent hidden semi-markov model, in: Proceedings of the Twenty-Seventh International Joint Conference on Artificial Intelligence, 2018, pp. 2447–2453.
- M. Fraccaro, S. K. Sønderby, U. Paquet, O. Winther, Sequential neural models with stochastic layers, *Advances in Neural Information Processing Systems* 29 (2016).
- A. Farnoosh, B. Azari, S. Ostadabbas, Deep switching auto-regressive factorization: Application to time series forecasting, in: Proceedings of the AAAI Conference on Artificial Intelligence, 8, 2021, pp. 7394–7403.
- Z. Dong, B. Seybold, K. Murphy, H. Bui, Collapsed amortized variational inference for switching nonlinear dynamical systems, in: International Conference on Machine Learning, 2020, pp. 2638–2647.
- S. Linderman, M. Johnson, A. Miller, R. Adams, D. Blei, L. Paninski, Bayesian learning and inference in recurrent switching linear dynamical systems, in: *Artificial Intelligence and Statistics*, 2017, pp. 914–922.
- P. Becker-Ehmck, J. Peters, P. Van Der Smagt, Switching linear dynamics for variational Bayes filtering, in: International Conference on Machine Learning, 2019, pp. 553–562.
- J. Nassar, S. Linderman, M. Bugallo, I. M. Park, Tree-structured recurrent switching linear dynamical systems for multi-scale modeling, in: International Conference on Learning Representations, 2018, pp. 1–9.
- R. Kurl, S. S. Rangapuram, E. de Bézenac, S. Günnemann, J. Gasthaus, Deep rao-blackwellised particle filters for time series forecasting, in: *Advances in Neural Information Processing Systems*, 2020, pp. 15371–15382.
- K. He, X. Zhang, S. Ren, J. Sun, Deep residual learning for image recognition, in: Proceedings of the IEEE Conference on Computer Vision and Pattern Recognition, 2016, pp. 770–778.
- A. Vaswani, N. Shazeer, N. Parmar, J. Uszkoreit, L. Jones, A. N. Gomez, L. u. Kaiser, I. Polosukhin, Attention is all you need, in: *Advances in Neural Information Processing Systems*, 2017, pp. 1–11.

- D. Geiger, T. Verma, J. Pearl, Identifying independence in bayesian networks, *Networks* 20 (1990) 507–534.
- R. J. Williams, Simple statistical gradient-following algorithms for connectionist reinforcement learning, *Machine Learning* 8 (1992) 229–256.
- P. Giudici, M. Mezzetti, P. Muliere, Mixtures of products of dirichlet processes for variable selection in survival analysis, *Journal of Statistical Planning and Inference* 111 (2003) 101–115.
- P. Giudici, T. Ryden, P. Vandekerkhove, Likelihood-ratio tests for hidden markov models, *Biometrics* 56 (2000) 742–747.
- X. Xu, Y. Chen, Y. Goude, Q. Yao, Probabilistic forecasting for daily electricity loads and quantiles for curve-to-curve regression, *Applied Energy* 301 (2021) 1–14.
- H. Cho, Y. Goude, X. Brossat, Q. Yao, Modeling and forecasting daily electricity load curves: A hybrid approach, *Journal of the American Statistical Association* 108 (2013) 7–21.
- F. X. Diebold, R. S. Mariano, Comparing predictive accuracy, *Journal of Business & Economic Statistics* 20 (2002) 134–144.
- G. Babaei, P. Giudici, E. Raffinetti, A rank graduation box for safe ai, *Expert Systems with applications* 259 (2025) 125239.
- S. P. Nandanoori, A. Diwadkar, U. Vaidya, Mean square stability analysis of stochastic continuous-time linear networked systems, *IEEE Transactions on Automatic Control* 63 (2018) 4323–4330.
- J. Drgona, S. Mukherjee, J. Zhang, F. Liu, M. Halappanavar, On the stochastic stability of deep markov models, *Advances in Neural Information Processing Systems* 34 (2021) 24033–24047.

Appendix A. Derivation of the evidence lower bound (ELBO)

The ELBO for the log-likelihood can be derived as follows:

$$\begin{aligned}
\mathcal{L}(\theta) &\geq \text{ELBO}(\theta, \phi) \\
&= \iint q_\phi(\mathbf{z}_{1:T}, \mathbf{d}_{1:T} | \mathbf{y}_{1:T}, \mathbf{x}_{1:T}) \log \frac{p_\theta(\mathbf{y}_{1:T}, \mathbf{z}_{1:T}, \mathbf{d}_{1:T} | \mathbf{x}_{1:T})}{q_\phi(\mathbf{z}_{1:T}, \mathbf{d}_{1:T} | \mathbf{y}_{1:T}, \mathbf{x}_{1:T})} d\mathbf{z}_{1:T} d\mathbf{d}_{1:T} \\
&= \iint q_\phi(\mathbf{z}_{1:T}, \mathbf{d}_{1:T} | \mathbf{y}_{1:T}, \mathbf{h}_{1:T}) \log \frac{p_\theta(\mathbf{y}_{1:T}, \mathbf{z}_{1:T}, \mathbf{d}_{1:T} | \mathbf{h}_{1:T})}{q_\phi(\mathbf{z}_{1:T}, \mathbf{d}_{1:T} | \mathbf{y}_{1:T}, \mathbf{h}_{1:T})} d\mathbf{z}_{1:T} d\mathbf{d}_{1:T} \\
&= \mathbb{E}_{q_\phi} [\log p_\theta(\mathbf{y}_{1:T} | \mathbf{z}_{1:T}, \mathbf{d}_{1:T}, \mathbf{h}_{1:T})] - \text{KL}(q_\phi(\mathbf{z}_{1:T}, \mathbf{d}_{1:T} | \mathbf{y}_{1:T}, \mathbf{h}_{1:T}) \| p_\theta(\mathbf{z}_{1:T}, \mathbf{d}_{1:T} | \mathbf{h}_{1:T})) \\
&= \mathbb{E}_{q_\phi} \left[\sum_t \log p_\theta(\mathbf{y}_t | \mathbf{z}_t, \mathbf{d}_t, \mathbf{h}_t) \right] - \int q_\phi(\mathbf{z}_{1:T}, \mathbf{d}_{1:T} | \mathbf{y}_{1:T}, \mathbf{h}_{1:T}) \log \frac{q_\phi(\mathbf{z}_{1:T}, \mathbf{d}_{1:T} | \mathbf{y}_{1:T}, \mathbf{h}_{1:T})}{p_\theta(\mathbf{z}_{1:T}, \mathbf{d}_{1:T} | \mathbf{h}_{1:T})} d\mathbf{z}_{1:T} d\mathbf{d}_{1:T} \\
&= \sum_t \mathbb{E}_{q_\phi} [\log p_\theta(\mathbf{y}_t | \mathbf{z}_t, \mathbf{d}_t, \mathbf{h}_t)] \\
&\quad - \sum_t \int q_\phi(\mathbf{z}_{1:T}, \mathbf{d}_{1:T} | \mathbf{y}_{1:T}, \mathbf{h}_{1:T}) \log \frac{q_{\phi_z}(\mathbf{z}_t | \mathbf{z}_{t-1}, \mathbf{d}_t, \mathbf{A}_t) q_{\phi_d}(\mathbf{d}_t | \mathbf{d}_{t-1}, \mathbf{A}_t)}{p_\theta(\mathbf{z}_t | \mathbf{z}_{t-1}, \mathbf{d}_t, \mathbf{h}_t) p_\theta(\mathbf{d}_t | \mathbf{d}_{t-1})} d\mathbf{z}_{1:T} d\mathbf{d}_{1:T} \\
&= \sum_t \mathbb{E}_{q_\phi} [\log p_\theta(\mathbf{y}_t | \mathbf{z}_t, \mathbf{d}_t, \mathbf{h}_t)] \\
&\quad - \sum_t \int q_\phi(\mathbf{z}_{1:T}, \mathbf{d}_{1:T} | \mathbf{y}_{1:T}, \mathbf{h}_{1:T}) \log \frac{q_{\phi_z}(\mathbf{z}_t | \mathbf{z}_{t-1}, \mathbf{d}_t, \mathbf{A}_t)}{p_\theta(\mathbf{z}_t | \mathbf{z}_{t-1}, \mathbf{d}_t, \mathbf{h}_t)} d\mathbf{z}_{1:T} d\mathbf{d}_{1:T} \\
&\quad - \sum_t \int q_\phi(\mathbf{z}_{1:T}, \mathbf{d}_{1:T} | \mathbf{y}_{1:T}, \mathbf{h}_{1:T}) \log \frac{q_{\phi_d}(\mathbf{d}_t | \mathbf{d}_{t-1}, \mathbf{A}_t)}{p_\theta(\mathbf{d}_t | \mathbf{d}_{t-1})} d\mathbf{z}_{1:T} d\mathbf{d}_{1:T} \\
&= \sum_t \mathbb{E}_{q_\phi^*(\mathbf{z}_t, \mathbf{d}_t)} [\log p_\theta(\mathbf{y}_t | \mathbf{z}_t, \mathbf{d}_t, \mathbf{h}_t)] \\
&\quad - \sum_t \mathbb{E}_{q_\phi^*(\mathbf{z}_{t-1}, \mathbf{d}_{t-1})} \int q_{\phi_z}(\mathbf{z}_t | \mathbf{z}_{t-1}, \mathbf{d}_t, \mathbf{A}_t) q_{\phi_d}(\mathbf{d}_t | \mathbf{d}_{t-1}, \mathbf{A}_t) \log \frac{q_{\phi_z}(\mathbf{z}_t | \mathbf{z}_{t-1}, \mathbf{d}_t, \mathbf{A}_t)}{p_\theta(\mathbf{z}_t | \mathbf{z}_{t-1}, \mathbf{d}_t, \mathbf{h}_t)} d\mathbf{z}_t d\mathbf{d}_t \\
&\quad - \sum_t \mathbb{E}_{q_\phi^*(\mathbf{d}_{t-2})} \int q_{\phi_d}(\mathbf{d}_{t-1} | \mathbf{d}_{t-2}, \mathbf{A}_{t-1}) q_{\phi_d}(\mathbf{d}_t | \mathbf{d}_{t-1}, \mathbf{A}_t) \log \frac{q_{\phi_d}(\mathbf{d}_t | \mathbf{d}_{t-1}, \mathbf{A}_t)}{p_\theta(\mathbf{d}_t | \mathbf{d}_{t-1})} d\mathbf{d}_t \\
&= \sum_t \mathbb{E}_{q_\phi^*(\mathbf{z}_{t-1}, \mathbf{d}_{t-1})} \mathbb{E}_{q_{\phi_z}(\mathbf{z}_t | \mathbf{z}_{t-1}, \mathbf{d}_t, \mathbf{A}_t)} \mathbb{E}_{q_{\phi_d}(\mathbf{d}_t | \mathbf{d}_{t-1}, \mathbf{A}_t)} [\log p_\theta(\mathbf{y}_t | \mathbf{z}_t, \mathbf{d}_t, \mathbf{h}_t)] \\
&\quad - \sum_t \mathbb{E}_{q_\phi^*(\mathbf{z}_{t-1}, \mathbf{d}_{t-1})} \mathbb{E}_{q_{\phi_d}(\mathbf{d}_t | \mathbf{d}_{t-1}, \mathbf{A}_t)} \text{KL}[q_{\phi_z}(\mathbf{z}_t | \mathbf{z}_{t-1}, \mathbf{d}_t, \mathbf{A}_t) \| p_\theta(\mathbf{z}_t | \mathbf{z}_{t-1}, \mathbf{d}_t, \mathbf{h}_t)] \\
&\quad - \sum_t \mathbb{E}_{q_\phi^*(\mathbf{d}_{t-2})} \mathbb{E}_{q_{\phi_d}(\mathbf{d}_{t-1} | \mathbf{d}_{t-2}, \mathbf{A}_{t-1})} \text{KL}[q_{\phi_d}(\mathbf{d}_t | \mathbf{d}_{t-1}, \mathbf{A}_t) \| p_\theta(\mathbf{d}_t | \mathbf{d}_{t-1})] \\
&= \sum_t \left\{ \mathbb{E}_{q_\phi^*(\mathbf{z}_{t-1}, \mathbf{d}_{t-1})} \sum_{\mathbf{d}_t} q_{\phi_d}(\mathbf{d}_t | \mathbf{d}_{t-1}, \mathbf{A}_t) \mathbb{E}_{q_{\phi_z}(\mathbf{z}_t | \mathbf{z}_{t-1}, \mathbf{d}_t, \mathbf{A}_t)} [\log p_\theta(\mathbf{y}_t | \mathbf{z}_t, \mathbf{d}_t, \mathbf{h}_t)] \right. \\
&\quad - \mathbb{E}_{q_\phi^*(\mathbf{z}_{t-1}, \mathbf{d}_{t-1})} \sum_{\mathbf{d}_t} q_{\phi_d}(\mathbf{d}_t | \mathbf{d}_{t-1}, \mathbf{A}_t) \text{KL}[q_{\phi_z}(\mathbf{z}_t | \mathbf{z}_{t-1}, \mathbf{d}_t, \mathbf{A}_t) \| p_\theta(\mathbf{z}_t | \mathbf{z}_{t-1}, \mathbf{d}_t, \mathbf{h}_t)] \\
&\quad \left. - \mathbb{E}_{q_\phi^*(\mathbf{d}_{t-2})} \sum_{\mathbf{d}_{t-1}} q_{\phi_d}(\mathbf{d}_{t-1} | \mathbf{d}_{t-2}, \mathbf{A}_{t-1}) \text{KL}[q_{\phi_d}(\mathbf{d}_t | \mathbf{d}_{t-1}, \mathbf{A}_t) \| p_\theta(\mathbf{d}_t | \mathbf{d}_{t-1})] \right\}
\end{aligned}$$

Appendix B. Stability analysis of DS³M

Theorem 1

DS³M exhibits latent state dynamics $z_t \sim N(\mu_{z,t}^{(d_t)}, \Sigma_{z,t}^{(d_t)})$, where the mean $\mu_{z,t}^{(d_t)}$ and the diagonal covariance matrix $\Sigma_{z,t}^{(d_t)}$ are parameterized by two neural network models $f_{z,1}^{(d_t)}$ and $f_{z,2}^{(d_t)}$. The latent variable z_t is globally stable in mean-square under the following conditions:

$$\|W_i^{f_{z,1}^{(d_t)}}\|_2 < 1, \quad \text{for } 1 \leq i \leq L_{f_{z,1}^{(d_t)}}, \quad (\text{B.1})$$

$$\|\mathcal{A}_i^{f_{z,1}^{(d_t)}}\|_2 \leq 1, \quad \text{for } 1 \leq i \leq L_{f_{z,1}^{(d_t)}} - 1, \quad (\text{B.2})$$

$$\|W_j^{f_{z,2}^{(d_t)}}\|_2 < 1, \quad \text{for } 1 \leq j \leq L_{f_{z,2}^{(d_t)}}, \quad (\text{B.3})$$

$$\|\mathcal{A}_j^{f_{z,2}^{(d_t)}}\|_2 \leq 1, \quad \text{for } 1 \leq j \leq L_{f_{z,2}^{(d_t)}} - 1. \quad (\text{B.4})$$

Similarly, for the observed time series, we model $y_t \sim \mathcal{N}(\mu_{y,t}^{(d_t)}, \Sigma_{y,t}^{(d_t)})$, where the mean $\mu_{y,t}^{(d_t)}$ and the covariance matrix $\Sigma_{y,t}^{(d_t)}$ are parameterized by neural networks $f_{y,1}^{(d_t)}$ and $f_{y,2}^{(d_t)}$, respectively. The observed variable y_t is globally stable in mean-square under the following conditions:

$$\|W_i^{f_{y,1}^{(d_t)}}\|_2 < 1, \quad \text{for } 1 \leq i \leq L_{f_{y,1}^{(d_t)}}, \quad (\text{B.5})$$

$$\|\mathcal{A}_i^{f_{y,1}^{(d_t)}}\|_2 \leq 1, \quad \text{for } 1 \leq i \leq L_{f_{y,1}^{(d_t)}} - 1, \quad (\text{B.6})$$

$$\|W_j^{f_{y,2}^{(d_t)}}\|_2 < 1, \quad \text{for } 1 \leq j \leq L_{f_{y,2}^{(d_t)}}, \quad (\text{B.7})$$

$$\|\mathcal{A}_j^{f_{y,2}^{(d_t)}}\|_2 \leq 1, \quad \text{for } 1 \leq j \leq L_{f_{y,2}^{(d_t)}} - 1. \quad (\text{B.8})$$

Here, $W_i^{f_{z,1}^{(d_t)}}$, $W_j^{f_{z,2}^{(d_t)}}$, $W_i^{f_{y,1}^{(d_t)}}$ and $W_j^{f_{y,2}^{(d_t)}}$ represent the weight matrices of neural networks $f_{z,1}^{(d_t)}$, $f_{z,2}^{(d_t)}$, $f_{y,1}^{(d_t)}$ and $f_{y,2}^{(d_t)}$, respectively; meanwhile, $\mathcal{A}_i^{f_{z,1}^{(d_t)}}$, $\mathcal{A}_j^{f_{z,2}^{(d_t)}}$, $\mathcal{A}_i^{f_{y,1}^{(d_t)}}$ and $\mathcal{A}_j^{f_{y,2}^{(d_t)}}$ denote their corresponding activation scaling matrices.

Proof:

Nandanoori et al. (2018) and Drgona et al. (2021) describes that a dynamic system is mean-square stable if its expected value and covariance converge

over time. That is, a time series $\mathbf{a}_t \in \mathbb{R}^n$ is stable if \mathbf{a}_t has $\lim_{t \rightarrow \infty} \mathbb{E}(\mathbf{a}_t) = \mu$ and $\lim_{t \rightarrow \infty} \mathbb{E}(\text{cov}(\mathbf{a}_t, \mathbf{a}_t)) = \Sigma$, in which $\mu \in \mathbb{R}$ and $\Sigma \in \mathbb{R}^n$.

Denote a neural network $f : \mathbb{R}^n \rightarrow \mathbb{R}^m$ parameterized by $\theta = \{W_0, \dots, W_L, b_0, \dots, b_L\}$ with hidden layers $1 \leq l \leq L$ with bias given as follows:

$$f_\theta(x) = W_L h_L + b_L \quad (\text{B.9})$$

$$h_l = a(W_{l-1} h_{l-1} + b_{l-1}) \quad (\text{B.10})$$

with $h_0 = x$, and $a : \mathbb{R}^k \rightarrow \mathbb{R}^k$ representing element-wise application of an activation function to vector elements such that $a(z) := [a(z_1) \dots a(z_k)]$.

Any neural network $f_\theta(x)$ with arbitrary activation functions—such as $f_{z,1}^{(d_t)}$, $f_{z,2}^{(d_t)}$, $f_{y,1}^{(d_t)}$, and $f_{y,2}^{(d_t)}$, which represent the means $\mu_{z,t}^{(d_t)}$ and $\mu_{y,t}^{(d_t)}$ and the diagonal covariance matrices $\Sigma_{z,t}^{(d_t)}$ and $\Sigma_{y,t}^{(d_t)}$ of latent or observed variables—can be equivalently expressed as a pointwise affine map:

$$\begin{aligned} f_\theta(x) &= W_L \mathcal{A}_{L-1} (W_{L-1} (\dots \mathcal{A}_1 (W_1 \mathcal{A}_0 (W_0 x + b_0) \\ &\quad + b_1) \dots) + b_{L-1}) + b_L \\ &= W_x x + b_x \end{aligned} \quad (\text{B.11})$$

where W_x and b_x are parametrized by input vector x :

$$W_x x = W_L \mathcal{A}_{L-1} W_{L-1} \dots \mathcal{A}_0 W_0 x \quad (\text{B.12})$$

$$\begin{aligned} b_x &= W_L \mathcal{A}_{L-1} \dots W_2 \mathcal{A}_1 W_1 \mathcal{A}_0 b_0 \\ &\quad + W_L \mathcal{A}_{L-1} \dots W_2 \mathcal{A}_1 b_1 + \dots \\ &\quad + W_L \mathcal{A}_{L-1} b_{L-1} + b_L \end{aligned} \quad (\text{B.13})$$

and \mathcal{A}_l represents parameter varying diagonal matrix of activation patterns.

We have shown that $f_{z,1}^{(d_t)}$ and $f_{z,2}^{(d_t)}$, with the latent variable z_{t-1} as part of their inputs, can be expressed in the form (B.11). Next, we prove that the latent variable z_t is globally stable in the mean-square sense, provided that conditions (B.1) to (B.4) are satisfied.

Assuming general non-square weights $W_i \in \mathbb{R}^{n_i \times m_i}$,

$$\|W_1 W_2 \dots W_m\|_2 \leq \|W_1\|_2 \cdot \|W_2\|_2 \dots \|W_m\|_2 \quad (\text{B.14})$$

holds because of the submultiplicativity of induced p-norms. Applying (B.14) to the linear parts (B.12) of the mean neural network $f_{z,1}^{(d_t)}$ in the equivalent pointwise affine form (B.11) with (B.1) and (B.2), it produces $\|W_i^{f_{z,1}^{(d_t)}}\|_2 < 1$

over the entire domain of $f_{z,1}^{(d_t)}(x)$. Since An affine map is a contraction if the 2-norm of its linear part is bounded below one, and Banach fixed-point theorem states that every contractive map converges towards single point equilibrium, $f_{z,1}^{(d_t)}$ is a contractive neural network and provides convergent mean $\mu_{z,t}^{(d_t)}$ for z_t as $t \rightarrow \infty$.

Similarly, using (B.14) to the linear parts (B.12) of the variance neural network $f_{z,2}^{(d_t)}$ in the equivalent pointwise affine form (B.11) with (B.3) and (B.4), it produces $\|W_x^{f_{z,2}^{(d_t)}}\|_2 < 1$. Hence, $f_{z,2}^{(d_t)}$ is a contractive neural network and provides convergent variance $\Sigma_{z,t}^{(d_t)}$ for z_t as $t \rightarrow \infty$. Therefore, z_t is globally mean-square stable when (B.1), (B.2), (B.3) and (B.4) are satisfied.

The observed time series is modeled as $y_t \sim \mathcal{N}(\mu_{y,t}^{(d_t)}, \Sigma_{y,t}^{(d_t)})$, where the mean $\mu_{y,t}^{(d_t)}$ and covariance matrix $\Sigma_{y,t}^{(d_t)}$ are parameterized by neural networks $f_{y,1}^{(d_t)}$ and $f_{y,2}^{(d_t)}$, respectively. These neural networks take the stable latent variable z_t as part of their inputs and are equivalent to pointwise affine maps (B.11). Using the same method employed to prove that z_t is globally mean-square stable, we can similarly show that y_t is globally stable in the mean-square sense if (B.5), (B.6), (B.7) and (B.8) are satisfied.

The constraints $\|\mathcal{A}_i^{f_{z,1}^{(d_t)}}\|_2 \leq 1$, $\|\mathcal{A}_j^{f_{z,2}^{(d_t)}}\|_2 \leq 1$, $\|\mathcal{A}_i^{f_{y,1}^{(d_t)}}\|_2 \leq 1$ and $\|\mathcal{A}_j^{f_{y,2}^{(d_t)}}\|_2 \leq 1$ on activation scaling matrices implies Lipschitz continuous activation functions with constants $k \leq 1$. In practice, DS³M satisfies these requirements by using ReLU (Rectified Linear Unit) activation functions.

Appendix C. Details on the hyperparameters of experiments

The DS³M is implemented in PyTorch and all experiments are conducted on a V100 GPU. As the sizes of the datasets are not large, a larger number of the hyperparameters does not lead to improvement of the performance. Therefore, we paid more attention to regularization methods during training instead of hyperparameter tuning. Specifically, we use Adam optimizer and the initial learning rate is set to 0.001 and is reduced by a factor of 0.1 when the validation loss has stopped improving for 10 epochs. An early stopping regularization is also implemented to stop the training when the validation loss has stopped improving for 20 epochs. All datasets are normalized before training and are transformed back for evaluation. The classical linear KL annealing approach is used to increase the coefficients of the KL terms from 0.01 to 1 over the course of the training process. Since 100 epochs are

sufficient for most experiments, we trained all models for 100 epochs during various evaluations. The number of switching states is set to 2. The batch size is set to 64. The dimension of the continuous latent variables is set to 2 for the toy example, the sleep apnea and the unemployment rate, 3 for the Lorenz, 50 for Pacific, and 10 for other datasets. All RNN are chosen to be 1-layer GRUs with the hidden dimension being 10 for the toy example, the sleep apnea and the unemployment rate, 20 for the Lorenz, 200 for the Pacific and the dimension of the observations D for other datasets. All MLPs are 2-layers with the hidden dimension to be the same as the dimension of the outputs. The hyperparameter of SNLDS and SRNN is chosen with the same rules and regularization methods. For the DSARF, we follow the same hyperparameters specified in Farnoosh et al. (2021). For the baseline simple GRU model, we use a grid search to fine-tune the parameters. The number of GRU layers is chosen in $[1, 2, 3, 4, 5]$, the hidden units are chosen from $[D, 2D, 3D, 4D, 5D]$. The model with the best validation loss is used to perform forecasting.